Journal of Molecular Liquids 269 (2018) 229–240

Contents lists available at ScienceDirect

Journal of Molecular Liquids

journal homepage: www.elsevier.com/locate/molliq

Heat transfer and entropy generation of the nanofluid flow inside sinusoidal wavy channels

Reza Dormohammadi [a,1], Mahmood Farzaneh-Gord [b,*], Amir Ebrahimi-Moghadam [a,1], Mohammad Hossein Ahmadi [a,*]

[a] Faculty of Mechanical Engineering, Shahrood University of Technology, Shahrood, Iran
[b] Faculty of Engineering, Mechanical Engineering Department, Ferdowsi University of Mashhad, Mashhad, Iran

ARTICLE INFO

Article history:
Received 16 June 2018
Received in revised form 28 July 2018
Accepted 31 July 2018
Available online 03 August 2018

Keywords:
Wavy channel
Sinusoidal wall
Nanofluid
Heat transfer
Entropy generation
Computational fluid dynamics (CFD)

ABSTRACT

Corrugating channel walls is a way to enhance heat transfer in heat exchangers. In the current investigation, the entropy generation minimization approach has been employed to optimize heat transfer and fluid flow within a wavy channel. A numerical method has been built to compute entropy generation rate in a sinusoidal wavy-wall channel with copper-water (Cu-water) nanofluid flow. The governing equations have been discretized using finite volume method for a two-dimensional steady flow. The effects of geometrical and flow parameters, including nanoparticles volume fraction ($0.01 < \phi < 0.05$), Richardson number ($0.1 < Ri < 10$), wave amplitude ratio ($0.1 < \alpha < 0.3$) and wave length ratio ($1 < \lambda < 3$), have been investigated. Results reveal that increasing nanoparticle volume fraction within investigated Richardson number will increase Nusselt number. In addition, the maximum entropy generation rate declines as Richarson number increases. The optimal wave amplitude ratio (corresponding to lowest entropy generation), for wave length ratios of $\lambda = 1$ and $\lambda = 2$, found to be $\alpha = 0.2$. Also, for wave length ratio of $\lambda = 3$, the minimum entropy generation approximately occurs at $\alpha = 0.1$.

1. Introduction

Employing wavy-wall channels is one way to enhance heat transfer [1,2] which are used in various systems such as heat exchangers [3–5], heat sinks [6] and solar collectors [7,8]. Accordingly, investigating heat transfer and fluid flow characteristics in wavy channels are one of the most interesting topics. Enhancing heat transfer is still an important issue in both of these categories. In addition of corrugation channel walls to increases heat transfer, the use of nanofluids in wavy channels also improves the existing conditions [9–11]. The nanofluids are composed of a base fluid component (such as water, oils and etc.) and nanoparticles (such as various metal oxides), in which the nanoparticles are dispersed in the base fluid [12–14].

The researches in the field of heat transfer and fluid flow characteristics in wavy channels can be classified into the two main categories based on the fluid flow: forced convection [15–19] and natural convection [20–24] heat transfer. In one of the recent studies on the use of nanofluids in corrugated channels, Nazari and Toghraie [25] investigated convective heat transfer in a porous sinusoidal channel filled with CuO-water nanofluid. They numerically solved the governing equations for a two-dimensional laminar flow. In another work, Akbarzadeh et al. [26] studied the effect of dispersing Cu nanoparticles to water for a corrugated channel. They employed finite volume method (FVM) for solving the governing equations and computed thermal and pumping power. Ahmed et al. [27] investigated the effect of the corrugation shape on the heat transfer enhancement for SiO_2-water nanofluid turbulent flow inside wavy channels numerically and experimentally. The same authors [28] also investigated the thermal–hydraulic performance of the laminar CuO-water nanofluid flow for various wavy channels. An experimental investigation was presented by Khoshvaght-Aliabadi and Sahamiyan [29] to examine the effects of the nanofluid mass flow rate, nanoparticle concentration and geometrical parameters on the heat transfer and pumping power for Al_2O_3-water flow inside the wavy minichannels. Khoshvaght-Aliabadi [30] also investigated the influence of the geometrical parameters of a sinusoidal wavy-wall channel on the heat transfer and friction factor for Al_2O_3-water nanofluid flow. He applied a numerical approach for simulating two-dimensional turbulent flow at different Reynolds numbers within the range of 6000–22,000. Nasrin et al. [31] investigated the accuracy of two different viscosity models on mixed convection heat transfer in a vertical lid driven cavity (with triangular corrugated walls) which was filled with CuO-water nanofluid. They used Galerkin's finite-element method to solve the governing equations. Sheremet et al. [32] proposed a numerical model for investigating free convection heat transfer for Cu-water

* Corresponding author.
E-mail addresses: m.farzanehgord@gmail.com (M. Farzaneh-Gord), mhosein.ahmadi@shahroodut.ac.ir (M.H. Ahmadi).
[1] These two authors contributed equally to this work.

https://doi.org/10.1016/j.molliq.2018.07.119
0167-7322/

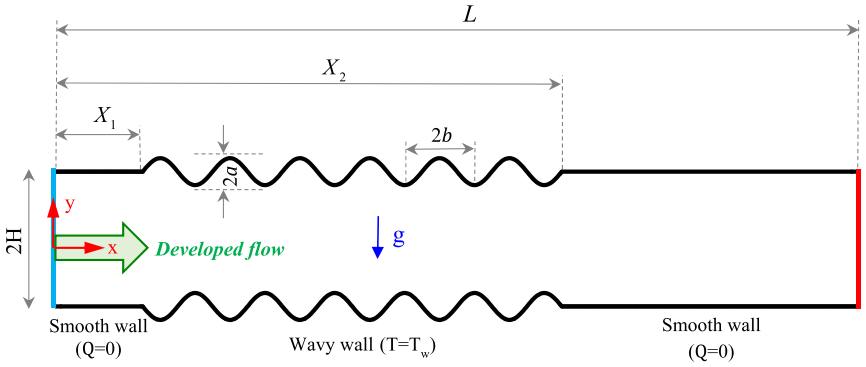

Fig. 1. Schematic diagram of the model under investigation.

nanofluid flow inside a cavity with wavy porous walls exposed to a magnetic field. Shenoy et al. [33] presented details of convective heat transfer inside wavy-wall channels for nanofluid flow.

To get more information about the quality of the available energy and also the optimal thermodynamic conditions of any systems, it is beneficial to calculate entropy generation [34–39]. Entropy generation minimization (EGM) approach can be also used for optimizing thermodynamic systems [40–50]. Similar to heat transfer studies, entropy generation investigation of wavy-wall channels could be also carried out for natural and forced convection. Sheremet et al. [51] employed CFD method to compute entropy generation in natural convection heat transfer of Cu-water nanofluid within a cavity with sinusoidal-corrugated vertical wall. In another work, Cho et al. [52] applied finite volume method for numerical modeling of free convective heat transfer and entropy generation for different metal oxide nanofluids (Cu-water, Al_2O_3-water, and TiO_2-water) in a horizontal enclosure with wavy walls.

The researches in the field of calculating the entropy generation amount for nanofluid flow inside horizontal wavy channels are very limited. In one of these limited studies, Akbarzadeh et al. [53] investigated heat transfer, pressure drop and entropy generation for cu-water nanofluid flow within a sinusoidal wavy-wall heat exchanger with a porous insert (the porous was inserted along the centerline of the heat exchanger). Akbarzadeh et al. [54] also studied a corrugated-wall solar heater numerically. By considering the Cu-water nanofluid turbulent flow, they investigated the effects of nanoparticles volume fraction and wall shapes (triangular, sinusoidal and straight ducts). In another work, Esfahani et al. [55] performed a two-dimensional numerical simulation (using Ansys-Fluent software) to calculate entropy generation of the Cu-water nanofluid flow in a wavy heat exchanger.

Based on the mentioned literature, most researches on the application of nanofluids in wavy channels have focused on the improvement of free convective heat transfer. In addition, a few researches have been carried out to utilize the entropy generation approach to optimize the design condition. Consequently, the aim of the present study is to improve (optimize) the mixed convective heat transfer for nanofluid flow inside a wavy channel using the entropy generation minimization approach. Cu–water nanofluid is chosen as working fluid due to its low cost and good heat transfer characteristic. The copper is a common material which could be prepared easily. From a variety of conventional wall corrugation shapes (such as triangular, trapezoidal, sinusoidal, etc.), the sinusoidal shape has been selected. As the first study on mixed convection nanofluid flow inside sinusoidal wavy channels, the effect of the nanoparticle volume fraction and geometry parameters (wave amplitude and wavelength) are investigated on heat transfer characteristics and entropy generation.

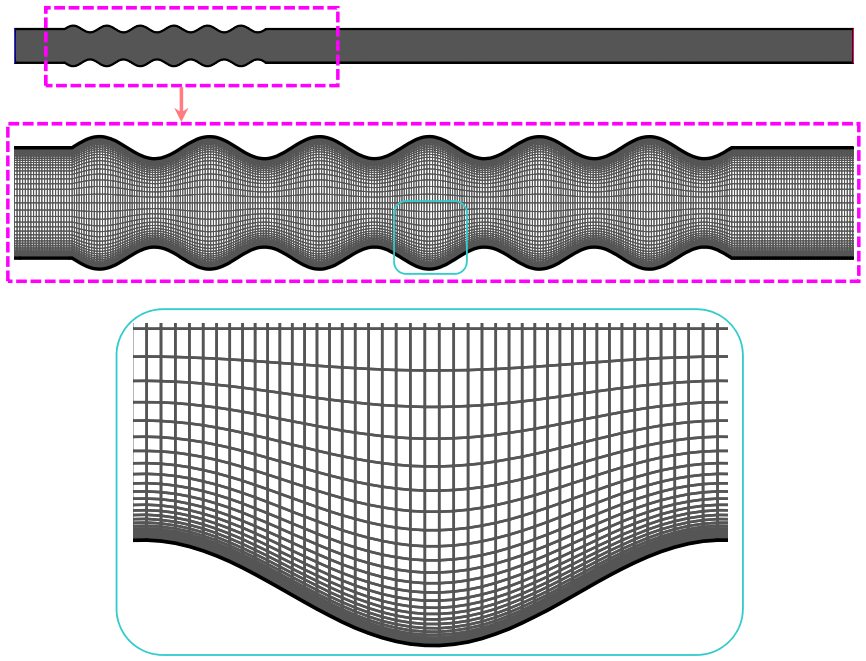

Fig. 2. Grid generation inside the computational domain and around the walls.

Table 1
Properties of investigated nanofluid in present study.

	Water	Cu
ρ (kg/m^3)	977.1	8954
C_p (J/kg.K)	4179	383
k (W/m.K)	0613	400
μ (N.s/m^2)	0.001	–
β (1/K) $\times 10^{-5}$	21	1.67

2. The numerical model and formulation

2.1. Geometry and grid generation

In this section, attention has been paid to introduce the case under investigation. Based on the previous researches [56,57], the sinusoidal corrugation walls causes better heat transfer and lower entropy generation in comparison to the other types of the wall corrugations (such as triangular and square). Consequently, the selected geometry is a sinusoidal wavy-wall channel with the total length of L and the height of $2H$. A schematic of the geometry is drawn in Fig. 1. As it can be seen, the channel is made of three sections: (1) the initial section ($0<x<X_1$) with smooth walls and adiabatic condition ($Q=0$), (2) the middle section ($X_1<x<X_2$) with sinusoidal walls and constant temperature condition ($T=T_w$), (3) the end section ($X_2<x<L$) with smooth walls and adiabatic condition ($Q=0$). The length of the initial and end sections are $X_1=3H$ and $X_1=15H$ from the origin. The sinusoidal curve is designed according to Eqs. (1) and (2). The wavy section has a wave amplitude of $2a$ and wave length of $2b$ and to express different geometries, the dimensionless parameters of the wave amplitude ratio $0.1<\alpha=a/H<0.3$ and the wave length ratio $1<\lambda=b/H<3$ are defined as dimensionless parameters.

$$S(x)=H+a\sin\left(\frac{\pi(x-X_1)}{H}\right):\text{top wavy-wall}\quad X_1<x<X_2 \tag{1}$$

$$S(x)=-H-a\sin\left(\frac{\pi(x-X_1)}{H}\right):\text{bottom wavy-wall}\quad X_1<x<X_2 \tag{2}$$

A sample grid generation of the computational domain and also a close-up view around walls is drawn in Fig. 2. The structured square meshes have been used for generating a high-quality grid. Due to the strong changes, higher mesh density is selected near the walls. This high-quality grid generation guarantees the accuracy of the calculations.

2.2. Governing equations

In present work, a two-dimensional, steady state, laminar, incompressible and viscous flow of Cu-water nanofluid inside a wavy channel is investigated. The governing equations for numerical simulation are containing continuity, momentum (in x and y directions) and energy equations; based on the above mentioned assumptions, these equations are defined as Eqs. (3) to (6), respectively [58–63].

$$\frac{\partial u}{\partial x}+\frac{\partial v}{\partial y}=0 \tag{3}$$

$$\rho_{nf}\left(u\frac{\partial u}{\partial x}+v\frac{\partial u}{\partial y}\right)=-\frac{\partial p}{\partial x}+\mu_{nf}\left(\frac{\partial^2 u}{\partial x^2}+\frac{\partial^2 u}{\partial y^2}\right) \tag{4}$$

$$\rho_{nf}\left(u\frac{\partial v}{\partial x}+v\frac{\partial v}{\partial y}\right)=-\frac{\partial p}{\partial y}+\mu_{nf}\left(\frac{\partial^2 v}{\partial x^2}+\frac{\partial^2 v}{\partial y^2}\right)+g(\rho\beta)_{nf}(T-T_c) \tag{5}$$

$$\rho_{nf}C_{nf}\left(u\frac{\partial T}{\partial x}+v\frac{\partial T}{\partial y}\right)=k_{nf}\left(\frac{\partial^2 T}{\partial x^2}+\frac{\partial^2 T}{\partial y^2}\right) \tag{6}$$

In which, u, v, p, T and g are velocity component in x direction, velocity component in y direction, pressure, temperature and gravity acceleration, respectively. Also, ρ_{nf}, μ_{nf}, β_{nf}, C_{nf} and k_{nf} represents density, viscosity, thermal expansion coefficient, heat capacity and conductively factor of the nanofluid, respectively. Determining the thermo-physical properties of the nanofluid is an important step in the modeling and the mentioned nanofluid thermo-physical properties are defined as following equations [64,65]:

$$\rho_{nf}=(1-\phi)\rho_f+\phi\rho_s \tag{7}$$

$$(\rho C)_{nf}=(1-\phi)(\rho C)_f+\phi(\rho C)_s \tag{8}$$

$$(\rho\beta)_{nf}=(1-\phi)(\rho\beta)_f+\phi(\rho\beta)_s \tag{9}$$

$$\mu_{nf}=\frac{\mu_f}{(1-\phi)^{2.5}} \tag{10}$$

$$\frac{k_{nf}}{k_f}=\frac{k_s+2k_f+2\phi(k_f-k_s)}{k_s+2k_f-\phi(k_f-k_s)} \tag{11}$$

In above equations, the f and s indexes refer to the base fluid and solid nanoparticles, respectively. In this research, water has been considered as the base fluid and copper nanoparticles have been selected as the solid part of the nanofluid. The base fluid is Newtonian and therefore all of the thermo-physical of the base fluid, except density, have been assumed to be constant and the density has been assumed to be changed linearly with temperature according to Boussinesq approximation. The Boussinesq formula is defined as Eq. (12) [66]. In this study, Prandtl number of the base fluid is equal to 6.82. Details of thermo-physical properties for liquid part (at reference temperature) and solid part of the nanofluid being considered in this research (water copper), are listed in Table 1.

$$\rho=\rho_0[1-\beta(T-T_0)] \tag{12}$$

In Eq. (12), ρ and ρ_0 are density of the base fluid at a desired temperature and the reference temperature, respectively. It should be noted that ρ_0 has a constant value at the reference temperature which is listed in Table 1.

2.3. Dimensionless form of governing equations

For better presenting the results, dimensionless form of parameters and equations were used. Hence, to obtain a dimensionless form of the governing equations, following dimensionless parameters were used.

Table 2
Effect of the computational cell number on the average Nusselt number (for $\phi=0$, $\alpha=0.2$, $Gr=10^4$ and $Ri=1$).

Geometry no.	Grid size	$Nu_{ave,\ top}$	Relative difference (%)	$Nu_{ave,\ bottom}$	Relative difference (%)
1	20 × 256	4.1032	**1.33**	4.0197	**2.32**
2	30 × 510	4.0486	**0.23**	3.9265	**0.06**
3	50 × 1022	4.0393	**0.04**	3.9241	**0.02**
4	60 × 2044	4.0377	–	3.9233	–

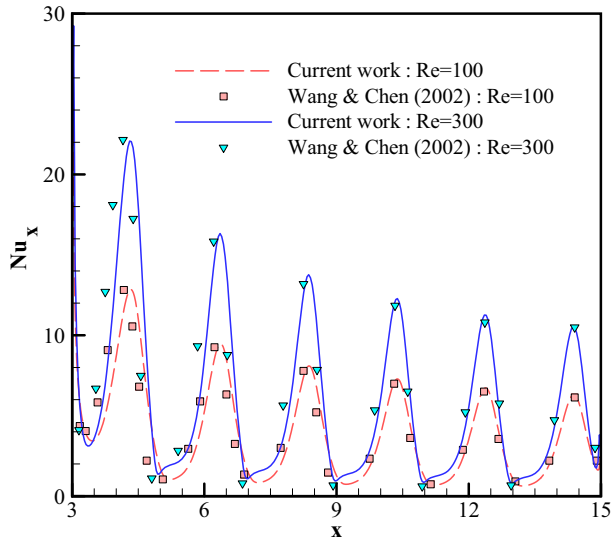

Fig. 3. Comparison of a local Nusselt number between current work and the other for α= 0.2 and different Reynolds numbers.

Some of the important dimensionless numbers used in this study are Reynolds number (Re), Grashof number (Gr), Prandtl number (Pr), and Richardson number (Ri), which are defined as:

$$X = \frac{x}{H}, \quad Y = \frac{y}{H}, \quad U = \frac{u}{U_0}, \quad V = \frac{v}{U_0} \tag{13}$$

$$P = \frac{p}{\rho_f U_0^2}, \quad \theta = \frac{T - T_0}{T_w - T_0} \tag{14}$$

$$\mathrm{Re} = \frac{U_0 \rho_f H}{\mu_f} \tag{15}$$

$$\mathrm{Gr} = \frac{g \beta_f H^3 (T_w - T_0)}{\upsilon_f^2} \tag{16}$$

$$\mathrm{Pr} = \frac{\upsilon_f}{\alpha_f} \tag{17}$$

$$\mathrm{Ri} = \frac{\mathrm{Gr}}{\mathrm{Re}^2} \tag{18}$$

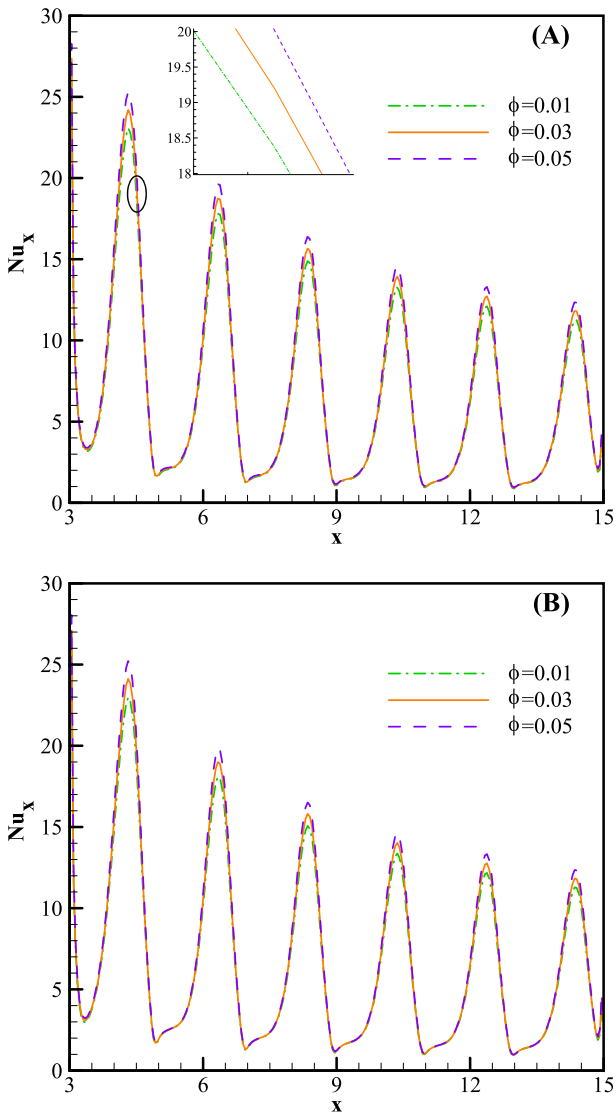

Fig. 4. Variation of the local Nusselt number along the wavy section for $\alpha = 0.2$, $\mathrm{Gr} = 10^4$ and Ri = 0.1, (A) bottom wall, (B) top wall.

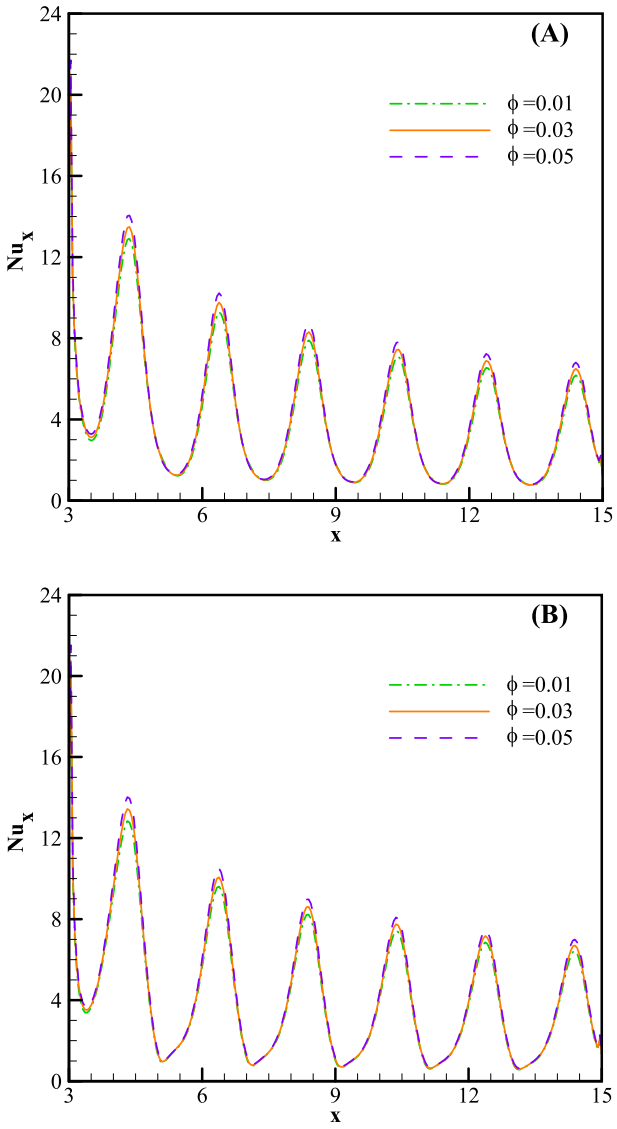

Fig. 5. Variation of the local Nusselt number along the wavy section for $\alpha = 0.2$, Gr = 104 and Ri = 1, (A) bottom wall, (B) top wall.

where, U_0, T_0 and T_w respectively indicates the average mean inlet velocity, inlet temperature and wall temperature. Considering mentioned dimensionless parameters, the dimensionless form of Eqs. (3) to (6) are re-written as Eqs. (19) to (22), respectively.

$$\frac{\partial U}{\partial X}+\frac{\partial V}{\partial Y}=0 \tag{19}$$

$$U\frac{\partial U}{\partial X}+V\frac{\partial U}{\partial Y}=\frac{\rho_f}{\rho_{nf}}\left[-\frac{\partial P}{\partial X}+\frac{1}{\mathrm{Re}}\frac{\mu_{nf}}{\mu_f}\left(\frac{\partial^2 U}{\partial X^2}+\frac{\partial^2 U}{\partial Y^2}\right)\right] \tag{20}$$

$$U\frac{\partial V}{\partial X}+V\frac{\partial V}{\partial Y}=\frac{\rho_f}{\rho_{nf}}\left[-\frac{\partial P}{\partial Y}+\frac{1}{\mathrm{Re}}\frac{\mu_{nf}}{\mu_f}\left(\frac{\partial^2 V}{\partial X^2}+\frac{\partial^2 V}{\partial Y^2}\right)+\frac{(\rho\beta)_{nf}}{(\rho\beta)_f}\mathrm{Ri}\theta\right] \tag{21}$$

$$U\frac{\partial \theta}{\partial X}+V\frac{\partial \theta}{\partial Y}=\frac{1}{\mathrm{Re}\cdot\ \mathrm{Pr}}\frac{k_{nf}}{k_f}\frac{(\rho C)_f}{(\rho C)_{nf}}\left(\frac{\partial^2 \theta}{\partial X^2}+\frac{\partial^2 \theta}{\partial Y^2}\right) \tag{22}$$

Table 3
Variation of the average Nusselt number in terms of Richardson number and nanoparticle volume fraction for $\alpha = 0.2$ and $\mathrm{Gr} = 10^4$.

		Nu_{ave}	
Ri	ϕ	Bottom wall	Top wall
0.1	0	6.3076	6.4621
	0.01	6.4465	6.5926
	0.02	6.5837	6.7213
	0.03	6.7183	6.8483
	0.04	6.8516	6.9744
	0.05	6.9836	7.0994
1	0	3.9241	4.0394
	0.01	4.0027	4.1193
	0.02	4.0826	4.1996
	0.03	4.1636	4.2803
	0.04	4.2460	4.3618
	0.05	4.3289	4.4433
10	0	2.5643	2.8633
	0.01	2.6173	2.9132
	0.02	2.6707	2.9637
	0.03	2.7245	3.0148
	0.04	2.7788	3.0668
	0.05	2.8333	3.1193

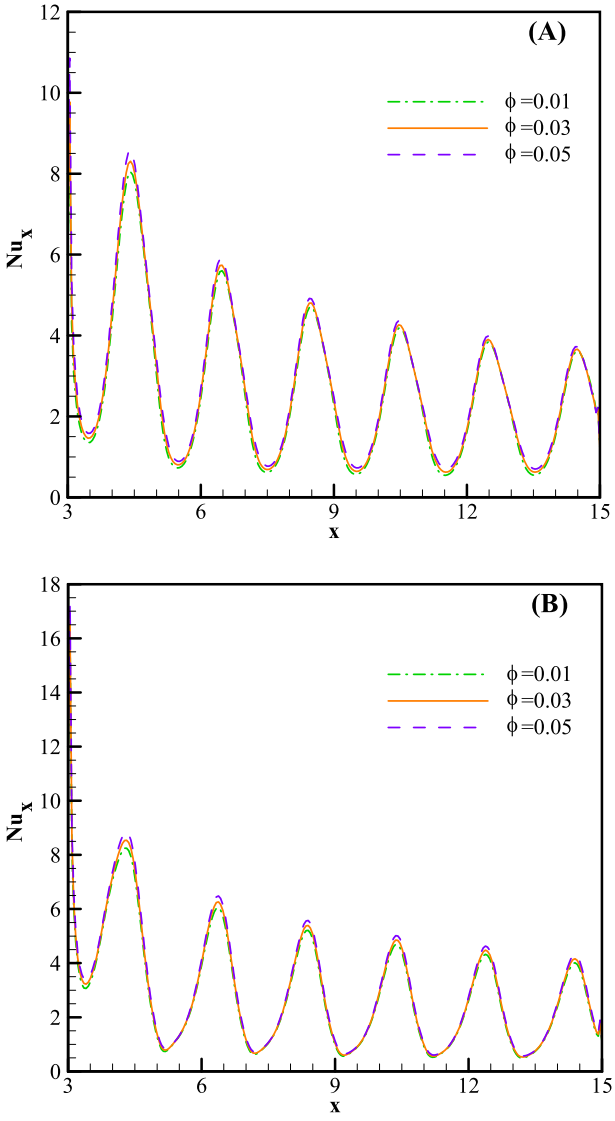

Fig. 6. Variation of the local Nusselt number along the wavy section for $\alpha = 0.2$, Gr = 104 and Ri = 10, (A) bottom wall, (B) top wall.

2.4. Boundary conditions

To solve the governing equations of the problem, following boundary conditions were assumed:

-*Inlet*:

In inlet boundary, for velocity field, the velocity profile was assumed as fully-developed and the inlet temperature was assumed to be constant ($T=T_0=300$ K). These conditions are presented in Eq. (23).

$$u=\frac{3}{2}U_0\left[1-\left(\frac{y}{H}\right)^2\right],\quad v=0,\quad T=T_0\ =300\ \mathrm{K} \tag{23}$$

-*Channel Walls*:

The no-slip condition was assumed for channel walls; also for smooth and wavy walls, adiabatic and constant temperature conditions were assumed, respectively.

$$u=0,\quad v=0,\quad T=T_w\ =310\ \mathrm{K}\quad \text{wavy walls} \tag{24}$$

$$u=0,\quad v=0,\quad \frac{\partial T}{\partial y}=0\quad \text{smooth walls} \tag{25}$$

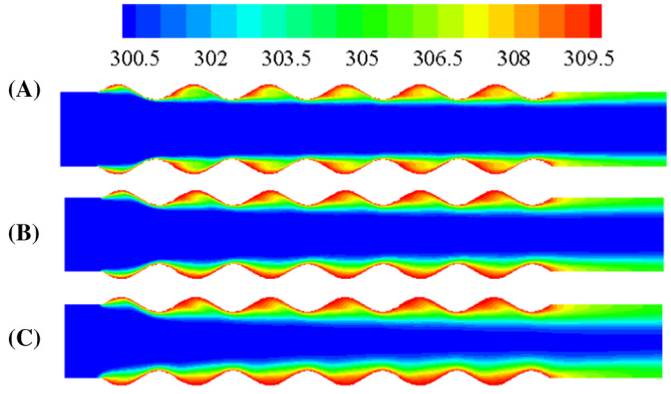

Fig. 7. Temperature contour plot for $\alpha = 0.2$ and $\mathrm{Gr} = 10^4$, (A) Ri = 0.1, (B) Ri = 1, (C) Ri = 10.

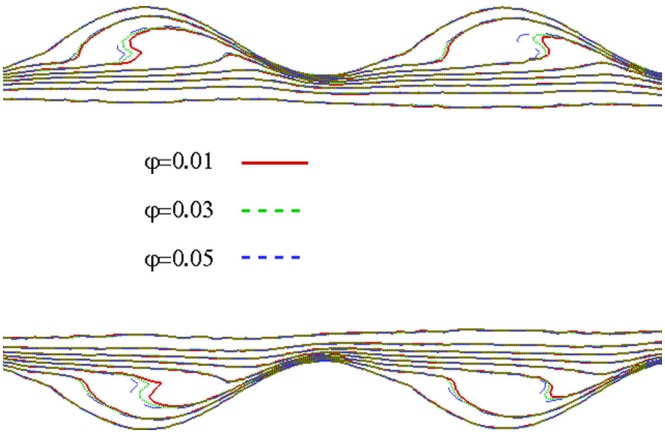

Fig. 8. Temperature distribution for $\alpha = 0.2$, $Gr = 10^4$ and $Ri = 0.1$ at various volume concentrations.

-*Outlet*:

On this boundary, the zero-gradient condition was assumed as:

$$\frac{\partial u}{\partial x} = 0, \quad \frac{\partial v}{\partial x} = 0, \quad \frac{\partial T}{\partial x} = 0 \tag{26}$$

It should be noted, the effect of Richardson number and volume fraction of the nanoparticles on quantities of heat transfer and entropy production was considered in the ranges of $0.1 < Ri < 10$ and $0.01 < \phi < 0.05$.

2.5. Numerical simulation process

The governing equations with mentioned boundary conditions were discretized and solved in Ansys-Fluent software using pressure-based finite volume method. A SIMPLE algorithm was used to establish the relation between velocity and pressure fields. The effects of the viscous dissipation and radiation heat transfer on the flow field and temperature field are ignored. Absolute convergence error of the residuals in order to stop the computations was assumed from 10^{-6} to 10^{-9} which guarantees the high accuracy of the results.

2.6. Heat transfer and entropy generation analysis

To investigate the extent of heat transfer, the dimensionless variable of the Nusselt number was used. Local and average Nusselt numbers are calculated using Eqs. (27) and (28), respectively.

$$Nu_x = -\frac{k_{nf}}{k_f}\frac{\partial \theta}{\partial n}\bigg|_{wall} \tag{27}$$

$$Nu_{avg} = \frac{1}{(X_2 - X_1)}\int_{X_1}^{X_2} Nu_x dx \tag{28}$$

In Eq. (27), n indicates the vector perpendicular to the corrugated surface.

Existence of irreversible resources, such as the effect of viscous and thermal dissipations, in the flow field results in entropy generation. The local volumetric entropy generation rate for two-dimensional flow is defined as Eq. (29). It should be noted that, the first term in Eq. (29) (S_H) shows the entropy generation due to heat transfer (thermal dissipations) and the second term (S_V) indicates entropy generation due to fluid flow (viscous dissipations) [23,67].

$$\dot{S}'''_{gen} = \dot{S}'''_{gen,H} + \dot{S}'''_{gen,V} = \frac{k_{nf}}{T^2}\left[\left(\frac{\partial T}{\partial x}\right)^2 + \left(\frac{\partial T}{\partial y}\right)^2\right] + \frac{\mu_{nf}}{T}\left[2\left(\frac{\partial u}{\partial x}\right)^2 + 2\left(\frac{\partial v}{\partial y}\right)^2 + \left(\frac{\partial u}{\partial y} + \frac{\partial v}{\partial x}\right)^2\right] \tag{29}$$

By applying the mentioned dimensionless parameters into Eq. (29), the local entropy generation number (a dimensionless form of the

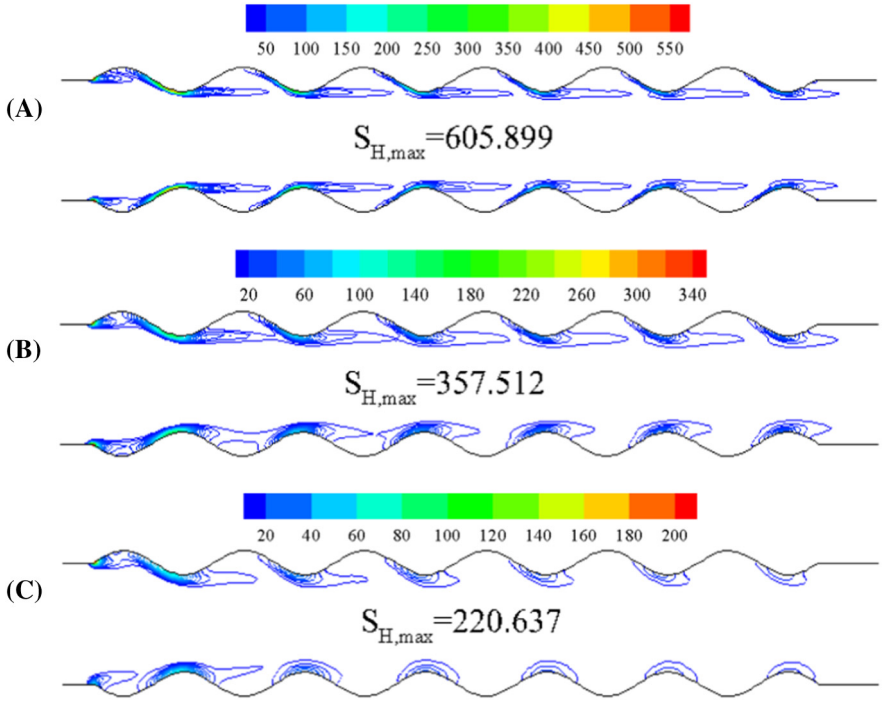

Fig. 9. Thermal entropy generation distribution for $\alpha = 0.2$ and $Gr = 10^4$, (A) $Ri = 0.1$, (B) $Ri = 1$, (C) $Ri = 10$.

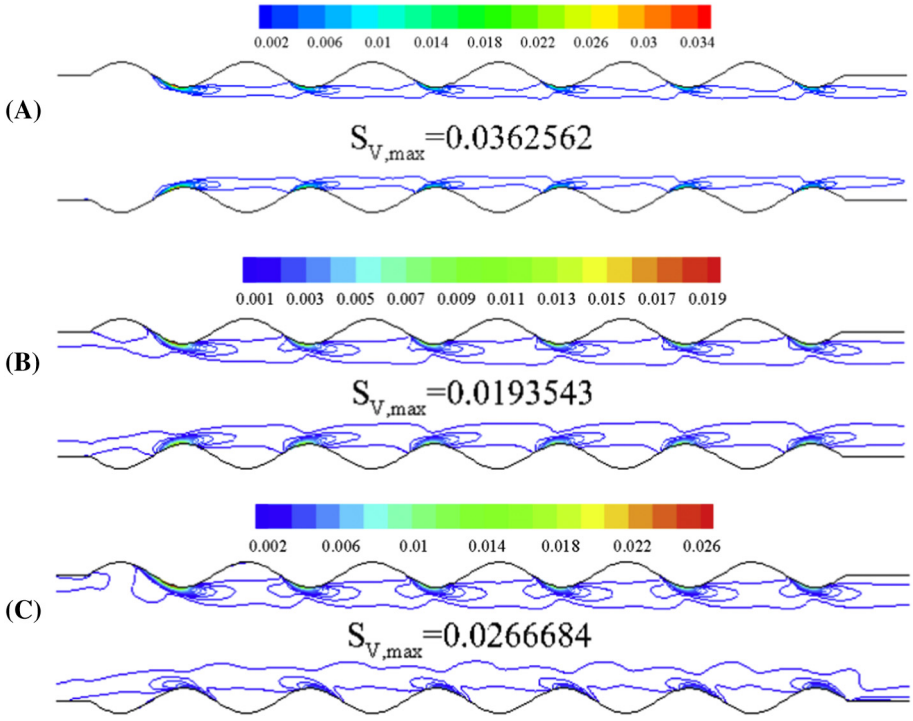

Fig. 10. Frictional entropy generation distribution for $\alpha = 0.2$ and $Gr = 10^4$, (A) Ri = 0.1, (B) Ri = 1, (C) Ri = 10.

entropy generation) can be written as Eq. (30).

$$N_g = \frac{k_{nf}}{k_f}\left[\left(\frac{\partial\theta}{\partial X}\right)^2 + \left(\frac{\partial\theta}{\partial Y}\right)^2\right] + \psi\frac{\mu_{nf}}{\mu_f}\left[2\left(\frac{\partial U}{\partial X}\right)^2 + 2\left(\frac{\partial V}{\partial Y}\right)^2 + \left(\frac{\partial U}{\partial Y} + \frac{\partial V}{\partial X}\right)^2\right] \quad (30)$$

In which, the parameter ψ is called irreversibility ratio factor and defined as Eq. (31). It is considered to be 10^{-4} in the current study.

$$\psi = \frac{\mu_f T_b}{k_f}\left(\frac{U_0}{T_w - T_b}\right)^2, \quad T_b = \frac{T_w + T_0}{2} \quad (31)$$

In which, T_b is bulk temperature and $\Delta T = T_w - T_b$ indicates the wall-bulk fluid temperature difference [67]. By integrating Eq. (30) over the whole of the solution domain, the amount of the average entropy generation number is calculated as Eq. (32).

$$N_s = N_{s,H} + N_{s,V} = \int N_g d\forall \quad (32)$$

Also in order to consider the share of each of the irreversibility in entropy generation, Bejan number was used which its local and average value are defined as Eqs. (33) and (34), respectively [68].

$$\mathrm{Be}_l = \frac{N_{g,H}}{N_g} = \frac{\dot{S}'''_{gen,H}}{\dot{S}'''_{gen}} \quad (33)$$

$$\mathrm{Be}_{avg} = \frac{N_{s,H}}{N_s} \quad (34)$$

3. Grid-independent study

To investigate grid independency, a number of computational cells were investigated as the solution domain. Four similar geometries with different cell numbers were used and the value of the average Nusselt number in these geometries were calculated and compared to each other. Variation of the average Nusselt number on the upper and lower corrugated walls are provided in Table 2, for $\phi = 0$, $\alpha = 0.2$, $Gr = 10^4$ and Ri = 1.

According to Table 2, the percentage of the relative difference between results of geometries 3 and 4 is <0.04 and for this reasons, geometry 3 is used as a computational domain for the analysis. This table is presented as a sample from various cases which were investigated for grid independence test. The results of investigating independence from a number of computational cells for other geometries indicate that approximately the same grid size can be extended for all other geometries.

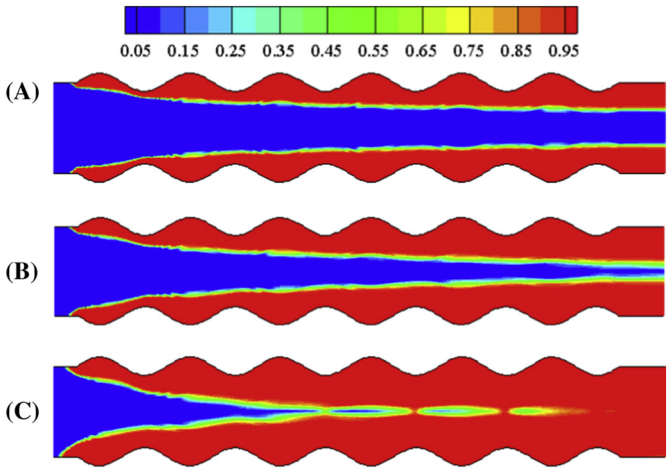

Fig. 11. Bejan number contour plot for $\alpha = 0.2$ and $Gr = 10^4$, (A) Ri = 0.1, (B) Ri = 1, (C) Ri = 10.

Table 4
Variation of the average Nusselt number in terms of wavelength ration and wave amplitude ratio for $\phi = 0.02$, $Gr = 10^4$ and $Ri = 1$.

Wavelength ratio	Wave amplitude ratio	Nu_{ave}	
λ	α	Bottom wall	Top wall
1	0.1	4.0599	4.1196
	0.2	3.5102	3.6373
	0.3	3.0932	3.2289
2	0.1	4.3443	4.3994
	0.2	4.0826	4.1996
	0.3	3.9925	4.4271
3	0.1	4.4195	4.4841
	0.2	4.2781	4.3166
	0.3	4.2041	4.5035

4. Model validation

To investigate the validity of the current numerical solution, the obtained results were compared with the results of Wang and Chen [69]. Wang and Chen [69] investigated forced convection in a wavy-wall channel numerically. The boundary conditions for model validation are assumed to be the same as the mentioned research. With the assumption of the small thermal expansion coefficient in a mixed convection study, forced convection would be made.

Variation of the local Nusselt number along the length of the wavy section of the channel for two Reynolds numbers is plotted in Fig. 3. According to Fig. 3, an acceptable conformity between this study and the results of the previous investigation is established. The figure indicates that the maximum amount of Nusselt number at the wavy section occurs at the beginning of the section (on the first wave). Also, by increasing the length of the wavy channel to a certain location along the x direction, the Nusselt number is decreasing; and from that location, by moving forward along the length of the channel, it can be seen that variation of the Nusselt number is negligible. For example, as it can be seen in Fig. 3, by increasing channel length prior to the third wave the Nusselt number declines and after that, variation of the Nusselt number with the length of the channel can be ignored.

5. Results and discussion

5.1. The effect of Richardson number

Figs. 4 to 6 show the local Nusselt number on top and bottom walls for varoiuse volume fractions at different Richardson numbers. According to these figures, by increasing nanoparticles volume fraction in the base fluid (water), the Nusselt number within wavy-wall section increases and consequently, the rate of the heat transfer through the two walls increases too. The mentioned changes observed for both the top and bottom walls. Since nanoparticles have a higher conduction heat transfer coefficient compared to the base fluid, increasing the volume fraction percentage of the nanoparticles causes an increase in conduction heat transfer and this leads to an increase in the heat transfer coefficient.

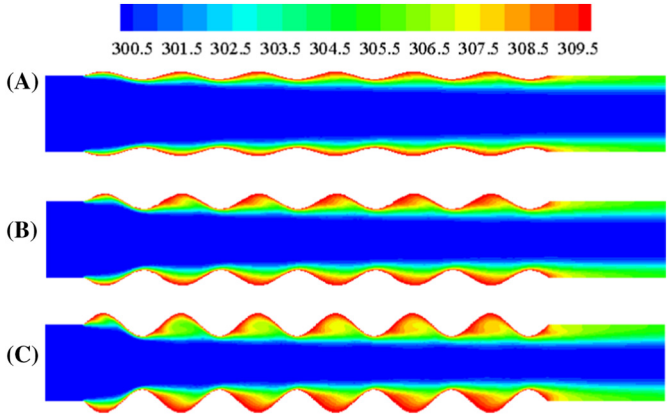

Fig. 13. Temperature contour plot for $\phi = 0.02$, $Gr = 10^4$, $Ri = 1$, $\lambda = 2$, (A) $\alpha = 0.1$, (B) $\alpha = 0.2$, (C) $\alpha = 0.3$.

Also, according to Figs. 4 to 6, changes in the average Nusselt number by increasing nanofluid volume fraction is significant at $Ri = 0.1$ compared to $Ri = 10$. Therefore, by increasing Richardson number from 0.1 to 10, the effect of nanoparticles addition into the base fluid would become less. Variation of the average Nusselt number in terms of Richardson number and nanoparticle volume fraction is presented in Table 3. According to this table, increasing nanoparticle volume fraction makes an increase in the average Nusselt number. As well as variation of the local Nusselt number, the results of this table (average Nusselt number) indicate an improvement in heat transfer by adding the nanoparticles. According to the definition of Richardson number, the mechanism of natural convection heat transfer would be promoted by increasing this number and consequently, its effects on general heat transfer is noticeable. For this reason, by increasing Richardson number, the difference in Nusselt numbers of the two walls will be increased.

Fig. 7 shows the effect of Richardson number on the temperature distribution for a certain geometry. According to this figure, at small Richardson numbers ($Ri = 0.1$), the isothermal lines are more contracted near the walls due to the predomination of the forced convective heat transfer mechanism (higher Reynolds Number). By increasing Richardson number, the natural convection in the general heat transfer is also incorporated and it causes an increase in the heat diffusion toward the central part of the channel. Also, according to this figure, it can be concluded that at higher Richardson numbers,

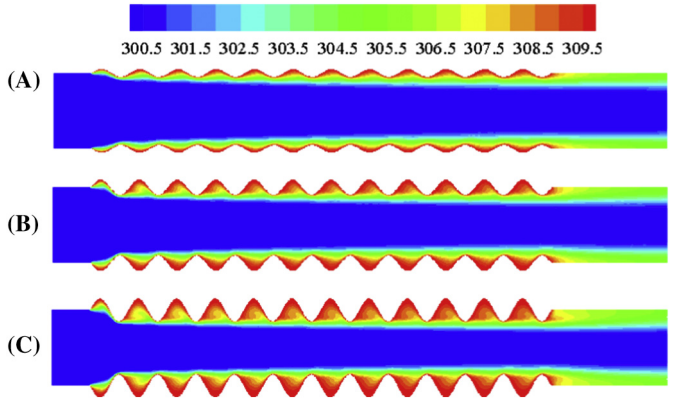

Fig. 12. Temperature contour plot for $\phi = 0.02$, $Gr = 10^4$, $Ri = 1$, $\lambda = 1$, (A) $\alpha = 0.1$, (B) $\alpha = 0.2$, (C) $\alpha = 0.3$.

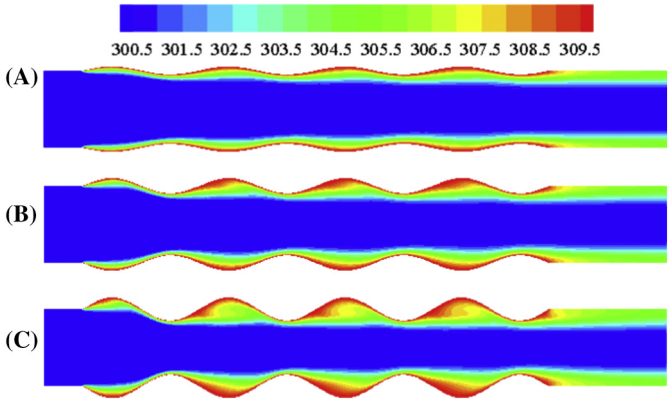

Fig. 14. Temperature contour plot for $\phi = 0.02$, $Gr = 10^4$, $Ri = 1$, $\lambda = 3$, (A) $\alpha = 0.1$, (B) $\alpha = 0.2$, (C) $\alpha = 0.3$.

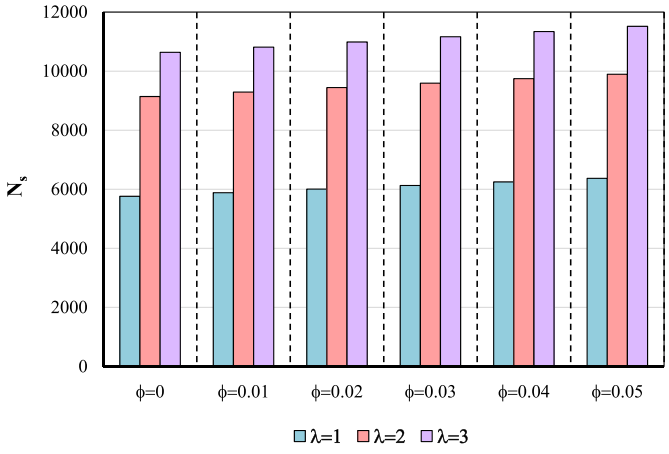

Fig. 15. Total entropy generation number in terms of volume fraction for Gr = 10^4, Ri = 1, $\alpha = 0.2$ and different wave length ratios.

asymmetry of the contours with respect to the central axis of the channel can be clearly observed. In the other words, considering symmetrical models (in all of the previous studies) causes errors at higher Richardson numbers.

Fig. 8 illustrates the temperature distribution inside the channel for different nanoparticle volume fractions. According to this figure, a variation of the volume fraction causes a trivial but effective difference in temperature distribution for mixed convective heat transfer inside the channel with corrugated walls.

The remaining part of the current section analyses the entropy generation of the problem under investigation. Fig. 9 depicts the distribution of entropy generation due to the heat transfer (thermal entropy generation). According to this figure, by increasing the Richardson number, the maximum entropy generation value decreases. It means that the natural convection heat transfer is improved by increasing the Richardson number. The maximum entropy generation relates to those regions with less area. In such regions, the thermal boundary layer is more compressed and heat transfer is increased. Fig. 10 illustrates the distribution of entropy generation due to the fluid flow (frictional entropy generation). At the smaller Richardson numbers, there will be higher velocities due to the dominance of forced convection. Accordingly, the velocity gradients near the walls are higher and frictional entropy generation is at its maximum level. From these figures, it can be concluded that the contribution of the thermal entropy generation in the total entropy generation is much greater than frictional entropy generation ($S_{gen,\,H} > > S_{gen,\,V}$).

Analyzing results reveals that by increasing volume fraction of nanoparticles at a certain Richardson number, both the thermal and frictional

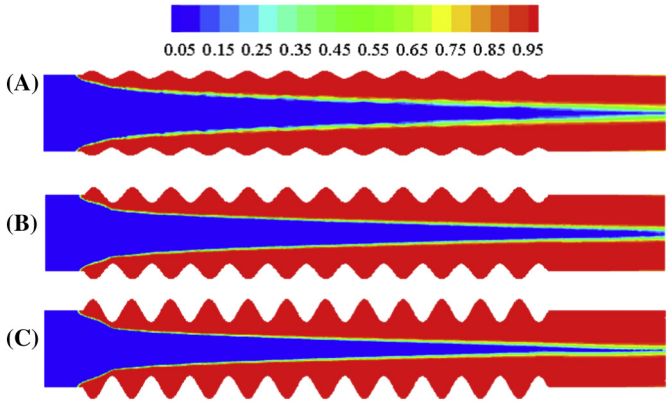

Fig. 16. Bejan number contour plot for $\phi = 0.02$, Gr = 10^4, Ri = 1, λ = 1, (A) $\alpha = 0.1$, (B) $\alpha = 0.2$, (C) $\alpha = 0.3$.

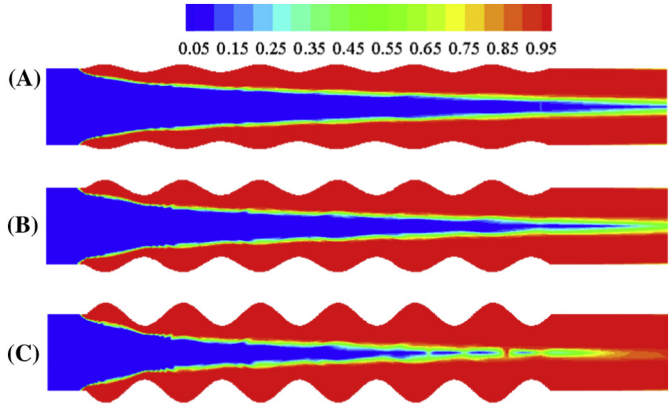

Fig. 17. Bejan number contour plot for $\phi = 0.02$, Gr = 10^4, Ri = 1, λ = 2, (A) $\alpha = 0.1$, (B) $\alpha = 0.2$, (C) $\alpha = 0.3$.

entropy generations are increased. As reported in Table 3, for a certain Richardson number, by increasing nanofluid volume fraction, the Nusselt number increases which means an increase in heat transfer. By increasing heat transfer, irreversibility due to heat transfer is increased which resulted to an increase in the thermal entropy generation. By increasing the nanofluid volume fraction, the effective viscosity of the fluid is increased and considering Eq. (30), frictional entropy generation is also increased.

In Fig. 11, the Bejan number contour plot is presented. According to this figure, by increasing Richardson number, the contribution of thermal entropy generation increases (Be > 0.5) inside the channel. As a result, the irreversibility due to heat transfer would become dominant. On the other hand, in the center of the channel, Bejan number is <0.5 (Be < 0.5) which means that the irreversibility due to fluid flow is more dominant in such regions.

5.2. The effect of wavelength and wave amplitude

To investigate the effect of the wave amplitude and wavelength on heat transfer, the average Nusselt numbers on top and bottom walls are provided in Table 4. According to this table, for all of the wavelength ratios, the amount of the average Nusselt number on bottom wall is decreased by increasing the wave amplitude ratio. On the other side, on the top wall, there is no uniform changes in the average Nusselt number in terms of wave amplitude ratio for higher wavelength ratios (λ = 2, 3); however, for lower wavelength ratios (λ = 1) the same decreasing trend in terms of wave amplitude ratio is also observed for Nusselt number on top wall. Also, based on Table 4, for all of the investigated wavelength ratios, the maximum heat transfer from the top wall is observed in the smallest wave amplitude ratio ($\alpha = 0.1$) and this has been proved

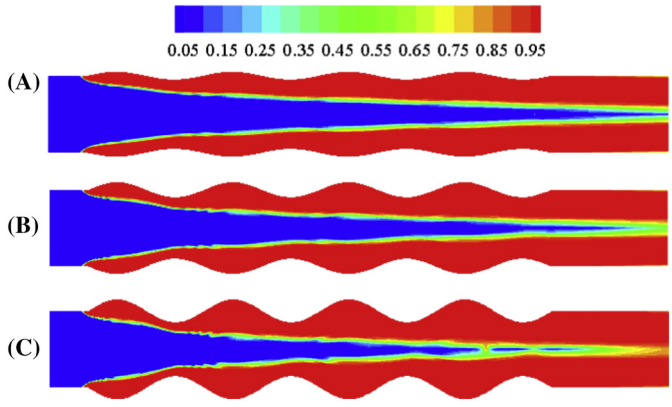

Fig. 18. Bejan number contour plot for $\phi = 0.02$, Gr = 10^4, Ri = 1, λ = 3, (A) $\alpha = 0.1$, (B) $\alpha = 0.2$, (C) $\alpha = 0.3$.

in Figs. 12 to 14. These figures illustrate temperature distribution inside the channel for different wave amplitude ratios and wavelengths ratios. According to these figures, for a specific wave length ratio, the heat transfer surface increases for $\alpha = 0.1$ and it results in an increase of the Nusselt number.

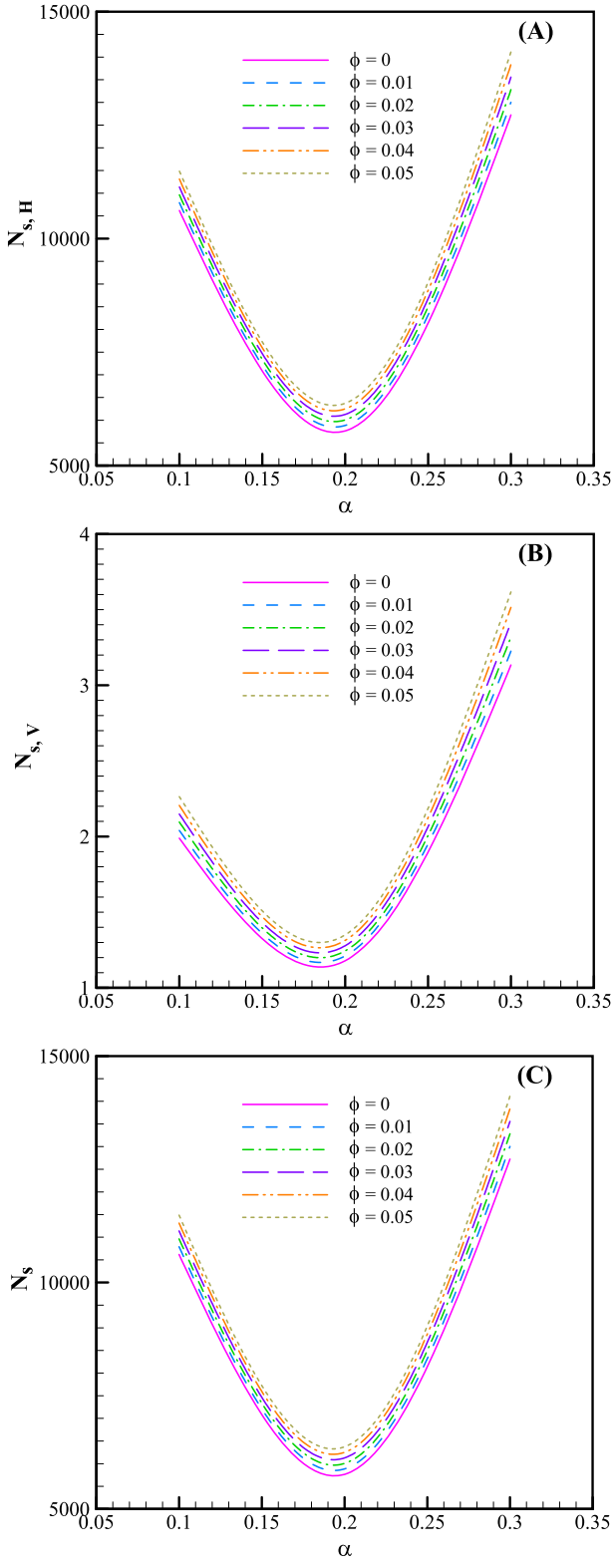

Fig. 19. Variation of, (A) thermal, (B) frictional, (C) total, entropy generation number in terms of wave amplitude ratio at different nanoparticle volume fractions for $Gr = 10^4$, $Ri = 1$ and $\lambda = 1$.

Analyzing the results showed that a reverse flow is created around the crest parts of each wave. This recirculation flow creates vortices at these regions. These vortices improve mixing of the nanofluid and thus increase the heat transfer within the channel. As the corners of the corrugated channel walls become sharper, the mentioned recirculating flow and vortices become stronger and therefore it causes an increase in heat transfer.

Fig. 15 shows average entropy generation number changes with nanoparticle volume fraction and wave amplitude ratio. According to this figure, in different wave amplitudes, total entropy generation increases by increasing nanoparticles concentration. Also, analyzing the results show that, for a certain wavelength and amplitude ratios, the total entropy generation varies as a linear function with nanoparticle volume fraction.

Figs. 16 to 18 depict the Bejan number contour plot for different wavelengths and wave amplitudes. According to these figures, in each wavelength ratio, by increasing amplitude ratio, the heat transfer contribution in entropy generation inside wavy channel decreased. Analyzing Figs. 16 to 18 and taking into account Eq. (33), it reveals that in a major part of the solution domain (especially near the walls), thermal entropy generation is the dominant portion of the total entropy generation. Also, from the channel walls toward the center of the channel, the proportion of the thermal entropy generation is reduced (near the channel centerline, the frictional entropy generation is the dominant term).

Variation of the thermal, frictional and total average entropy generation number in terms of wave amplitude for base fluid and different nanofluid volume fractions is presented in Fig. 19A–C, respectively. Results show that there is a point in which the entropy generation is minimum. As it is known, the less entropy generation corresponded to the more thermodynamically optimized system. According to Fig. 19, there is an optimal wave amplitude ratio for each wavelength ratio which occurs between 0.15 and 0.2. It is recommended to select a geometry with $\lambda = 1$ and $\alpha = 0.2$ to have the optimal conditions based on the lower entropy generation and higher heat transfer performance together. Also, based on Fig. 19, the optimal geometry selection does not depend on nanoparticle concentration but it has an effect on the amount of the entropy generation.

As it mentioned in previous sections, the order-of-magnitude of the thermal entropy generation is much greater than that frictional one ($N_{s,H} >> N_{s,V}$). It means that the total entropy generation is approximately equal to the thermal entropy generation ($N_s \approx N_{s,H}$).

Considering Eq. (11), it can be deduced that the adding nanoparticles into the base fluid (increasing ϕ) increase the thermal conductivity of the nanofluid. Assuming the other parameters are kept constant and considering the relation $h_{nf} = k_{nf}\frac{Nu_{nf}}{D_h}$, it can be concluded that adding nanoparticles increases the heat transfer and it leads to an increase in thermal entropy generation based on Eq. (29). On the other side, increasing nanoparticle volume fraction causes an increase in the fluid flow friction and it raises frictional entropy generation. Fig. 19A and B supports all these discussions.

6. Conclusion

In the present work, the effect of the geometrical parameters and nanoparticles dispersing into base fluid on the heat transfer characteristics and entropy generation inside a sinusoidal wavy-wall channel was investigated numerically. A two-dimensional CFD simulation was developed for modeling steady, incompressible and laminar flow of Cu-water nanofluid flow within the channel. Employing non-dimensional parameters, wave amplitude ratio, wavelength ratio, Richardson number and nanoparticles volume fraction, the following conclusions were observed:

- The heat transfer enhances by increasing the nanoparticles concentration in the investigated range of the Richardson number ($0.1 < Ri < 10$)

for both bottom and top walls. Also, a variation of the average Nusselt number by increasing nanofluid volume fraction is significant at lower Richardson number.

- At a specific wavelength ratio, increasing wave amplitude ratio for $0.1 < \alpha < 0.3$ causes a decrease in the bottom wall Nusselt number. On the other side, for the top wall, there is no uniform change of the average Nusselt number in terms of wave amplitude ratio and this implies that considering axisymmetric models causes errors from the real situation.
- The total entropy generation increases with reducing Richardson number and increasing nanoparticles concentration. For example, for a geometry with $\lambda = 1$ and $\alpha = 0.2$, increasing nanoparticle volume fraction from $\phi = 0.01$ to $\phi = 0.05$, a 6.5% increment is occurred in total entropy generation. Also, at a certain conditions, the order of magnitude of the thermal entropy generation is much higher than that frictional one ($S_{gen,\,H} >> S_{gen,\,V}$).
- The share of the heat transfer in entropy generation reduces by increasing the wave amplitude ratio at a specific wavelength ratio. In the other word, by increasing wave amplitude ratio, the thermal entropy generation and frictional entropy generation are increased and reduced, respectively.
- As a final result, designing a sinusoidal wavy channel with $\lambda = 1$ and $\alpha = 0.2$ can be applicable as an optimal wavy-wall heat exchanger (by considering both of the heat transfer and entropy generation together).

References

[1] T. Ma, L. Du, N. Sun, M. Zeng, B. Sundén, Q. Wang, Experimental and numerical study on heat transfer and pressure drop performance of Cross-Wavy primary surface channel, Energy Convers. Manag. 125 (2016) 80–90, https://doi.org/10.1016/j.enconman.2016.06.055.

[2] J. Rostami, A. Abbassi, J. Harting, Heat transfer by nanofluids in wavy microchannels, Adv. Powder Technol. 29 (2018) 925–933, https://doi.org/10.1016/j.apt.2018.01.010.

[3] X.W. Zhu, Y.H. Fu, J.Q. Zhao, A novel wavy-tape insert configuration for pipe heat transfer augmentation, Energy Convers. Manag. 127 (2016) 140–148, https://doi.org/10.1016/j.enconman.2016.09.006.

[4] M. Khoshvaght-Aliabadi, S. Davoudi, M.H. Dibaei, Performance of agitated-vessel U tube heat exchanger using spiky twisted tapes and water based metallic nanofluids, Chem. Eng. Res. Des. 133 (2018) 26–39, https://doi.org/10.1016/j.cherd.2018.02.030.

[5] M. Khoshvaght-Aliabadi, M. Tatari, M. Salami, Analysis on Al_2O_3/water nanofluid flow in a channel by inserting corrugated/perforated fins for solar heating heat exchangers, Renew. Energy 115 (2018) 1099–1108, https://doi.org/10.1016/j.renene.2017.08.092.

[6] M. Khoshvaght-Aliabadi, S.M. Hassani, S.H. Mazloumi, Performance enhancement of straight and wavy miniature heat sinks using pin-fin interruptions and nanofluids, Chem. Eng. Process. Process Intensif. 122 (2017) 90–108, https://doi.org/10.1016/j.cep.2017.10.002.

[7] M. Hatami, D. Jing, Evaluation of wavy direct absorption solar collector (DASC) performance using different nanofluids, J. Mol. Liq. 229 (2017) 203–211, https://doi.org/10.1016/j.molliq.2016.12.072.

[8] M. Hatami, D. Jing, Optimization of wavy direct absorber solar collector (WDASC) using Al_2O_3-water nanofluid and RSM analysis, Appl. Therm. Eng. 121 (2017) 1040–1050, https://doi.org/10.1016/j.applthermaleng.2017.04.137.

[9] M.H. Ahmadi, M.A. Ahmadi, M.A. Nazari, O. Mahian, R. Ghasempour, A proposed model to predict thermal conductivity ratio of Al_2O_3/EG nanofluid by applying least squares support vector machine (LSSVM) and genetic algorithm as a connectionist approach, J. Therm. Anal. Calorim. (2018)https://doi.org/10.1007/s10973-018-7035-z.

[10] A. Baghban, F. Pourfayaz, M.H. Ahmadi, A. Kasaeian, S.M. Pourkiaei, G. Lorenzini, Connectionist intelligent model estimates of convective heat transfer coefficient of nanofluids in circular cross-sectional channels, J. Therm. Anal. Calorim. 132 (2018) 1213–1239, https://doi.org/10.1007/s10973-017-6886-z.

[11] M.H. Ahmadi, M. Alhuyi Nazari, R. Ghasempour, H. Madah, M.B. Shafii, M.A. Ahmadi, Thermal conductivity ratio prediction of Al_2O_3/water nanofluid by applying connectionist methods, Colloids Surf. A Physicochem. Eng. Asp. 541 (2018) 154–164, https://doi.org/10.1016/j.colsurfa.2018.01.030.

[12] M.A. Nazari, R. Ghasempour, M.H. Ahmadi, G. Heydarian, M. Shafii, Experimental investigation of graphene oxide nanofluid on heat transfer enhancement of pulsating heat pipe, Int. Commun. Heat Mass Transfer 91 (2018) 90–94, https://doi.org/10.1016/j.icheatmasstransfer.2017.12.006.

[13] M.H. Ahmadi, A. Mirlohi, M.A. Nazari, R. Ghasempour, A review of thermal conductivity of various nanofluids, J. Mol. Liq. 265 (2018) 181–188, https://doi.org/10.1016/j.molliq.2018.05.124.

[14] N. Ijaz, A. Zeeshan, M.M. Bhatti, R. Ellahi, Analytical study on liquid-solid particles interaction in the presence of heat and mass transfer through a wavy channel, J. Mol. Liq. 250 (2018) 80–87, https://doi.org/10.1016/j.molliq.2017.11.123.

[15] S. Pati, S.K. Mehta, A. Borah, Numerical investigation of thermo-hydraulic transport characteristics in wavy channels: comparison between raccoon and serpentine channels, Int. Commun. Heat Mass Transfer 88 (2017) 171–176, https://doi.org/10.1016/j.icheatmasstransfer.2017.09.001.

[16] E. Aslan, I. Taymaz, Y. Islamoglu, Finite volume simulation for convective heat transfer in wavy channels, Heat Mass Transf. 52 (2016) 483–497, https://doi.org/10.1007/s00231-015-1571-x.

[17] P. Valinataj-Bahnemiri, A. Ramiar, S.A. Manavi, A. Mozaffari, Heat transfer optimization of two phase modeling of nanofluid in a sinusoidal wavy channel using Artificial Bee Colony technique, Eng. Sci. Technol. Int. J. 18 (2015) 727–737, https://doi.org/10.1016/j.jestch.2015.05.005.

[18] N. Shehzad, A. Zeeshan, R. Ellahi, K. Vafai, Convective heat transfer of nanofluid in a wavy channel: Buongiorno's mathematical model, J. Mol. Liq. 222 (2016) 446–455, https://doi.org/10.1016/j.molliq.2016.07.052.

[19] K.A. Mohammed, A.R. Abu Talib, A.A. Nuraini, K.A. Ahmed, Review of forced convection nanofluids through corrugated facing step, Renew. Sust. Energ. Rev. 75 (2017) 234–241, https://doi.org/10.1016/j.rser.2016.10.067.

[20] W. Tang, M. Hatami, J. Zhou, D. Jing, Natural convection heat transfer in a nanofluid-filled cavity with double sinusoidal wavy walls of various phase deviations, Int. J. Heat Mass Transf. 115 (2017) 430–440, https://doi.org/10.1016/j.ijheatmasstransfer.2017.07.057.

[21] M.A. Sheremet, D.S. Cimpean, I. Pop, Free convection in a partially heated wavy porous cavity filled with a nanofluid under the effects of Brownian diffusion and thermophoresis, Appl. Therm. Eng. 113 (2017) 413–418, https://doi.org/10.1016/j.applthermaleng.2016.11.033.

[22] K. Milani Shirvan, R. Ellahi, M. Mamourian, M. Moghiman, Effects of wavy surface characteristics on natural convection heat transfer in a cosine corrugated square cavity filled with nanofluid, Int. J. Heat Mass Transf. 107 (2017) 1110–1118, https://doi.org/10.1016/j.ijheatmasstransfer.2016.11.022.

[23] S. Mahmud, A.K.M.S. Islam, Laminar free convection and entropy generation inside an inclined wavy enclosure, Int. J. Therm. Sci. 42 (2003) 1003–1012, https://doi.org/10.1016/S1290-0729(03)00076-0.

[24] S. Mahmud, R. Fraser, Free Convection and Entropy Generation Inside a Vertical Inphase Wavy Cavity, vol. 31, 2004https://doi.org/10.1016/S0735-1933(04)00027-2.

[25] S. Nazari, D. Toghraie, Numerical simulation of heat transfer and fluid flow of Water-CuO Nanofluid in a sinusoidal channel with a porous medium, Phys. E Low-Dimensional Syst. Nanostructures 87 (2017) 134–140, https://doi.org/10.1016/j.physe.2016.11.035.

[26] M. Akbarzadeh, S. Rashidi, M. Bovand, R. Ellahi, A sensitivity analysis on thermal and pumping power for the flow of nanofluid inside a wavy channel, J. Mol. Liq. 220 (2016) 1–13, https://doi.org/10.1016/j.molliq.2016.04.058.

[27] M.A. Ahmed, M.Z. Yusoff, K.C. Ng, N.H. Shuaib, Numerical and experimental investigations on the heat transfer enhancement in corrugated channels using SiO_2–water nanofluid, Case Stud. Therm. Eng. 6 (2015) 77–92, https://doi.org/10.1016/j.csite.2015.07.003.

[28] M.A. Ahmed, M.Z. Yusoff, K.C. Ng, N.H. Shuaib, Effect of corrugation profile on the thermal–hydraulic performance of corrugated channels using CuO–water nanofluid, Case Stud. Therm. Eng. 4 (2014) 65–75, https://doi.org/10.1016/j.csite.2014.07.001.

[29] M. Khoshvaght-Aliabadi, M. Sahamiyan, Performance of nanofluid flow in corrugated minichannels heat sink (CMCHS), Energy Convers. Manag. 108 (2016) 297–308, https://doi.org/10.1016/j.enconman.2015.11.026.

[30] M. Khoshvaght-Aliabadi, Influence of different design parameters and Al_2O_3-water nanofluid flow on heat transfer and flow characteristics of sinusoidal-corrugated channels, Energy Convers. Manag. 88 (2014) 96–105, https://doi.org/10.1016/j.enconman.2014.08.042.

[31] R. Nasrin, M.A. Alim, A.J. Chamkha, Combined convection flow in triangular wavy chamber filled with water–CuO nanofluid: effect of viscosity models, Int. Commun. Heat Mass Transfer 39 (2012) 1226–1236, https://doi.org/10.1016/j.icheatmasstransfer.2012.06.005.

[32] M.A. Sheremet, H.F. Oztop, I. Pop, K. Al-Salem, MHD free convection in a wavy open porous tall cavity filled with nanofluids under an effect of corner heater, Int. Commun. Heat Mass Transfer 103 (2016) 955–964, https://doi.org/10.1016/j.ijheatmasstransfer.2016.08.006.

[33] A. Shenoy, M. Sheremet, I. Pop, Convective Flow and Heat Transfer from Wavy Surfaces: Viscous Fluids, Porous Media, and Nanofluids, CRC Press, 2016.

[34] C. Wu, L. Chen, J. Chen, Recent Advances in Finite-Time Thermodynamics, Nova Science Publishers, New York, 1999.

[35] L. Chen, F. Sun, Advances in Finite Time Thermodynamics: Analysis and Optimization, Nova Science Publishers, New York, 2004.

[36] C. Lingen, W. Chih, S. Fengrui, Finite time thermodynamic optimization or entropy generation minimization of energy systems, J. Non-Equilib. Thermodyn. 24 (1999) 327–359, https://doi.org/10.1515/JNETDY.1999.020.

[37] L. Chen, F. Meng, F. Sun, Thermodynamic analyses and optimization for thermoelectric devices: the state of the arts, Sci. China Technol. Sci. 59 (2016) 442–455.

[38] Y. Ge, L. Chen, F. Sun, Progress in finite time thermodynamic studies for internal combustion engine cycles, Entropy 18 (2016)https://doi.org/10.3390/e18040139.

[39] M.A. Sheremet, H.F. Oztop, I. Pop, N. Abu-Hamdeh, Analysis of entropy generation in natural convection of nanofluid inside a square cavity having hot solid block: Tiwari and Das' Model, Entropy 18 (2016)https://doi.org/10.3390/e18010009.

[40] L. Chen, L. Zhang, S. Xia, F. Sun, Entropy generation minimization for CO_2 hydrogenation to light olefins, Energy 147 (2018) 187–196, https://doi.org/10.1016/j.energy.2018.01.050.

[41] L. Chen, S. Xia, F. Sun, Entropy generation minimization for isothermal crystallization processes with a generalized mass diffusion law, Int. J. Heat Mass Transf. 116 (2018) 1–8, https://doi.org/10.1016/j.ijheatmasstransfer.2017.09.001.
[42] L. Chen, S. Xia, F. Sun, Optimal paths for minimizing entropy generation during heat transfer processes with a generalized heat transfer law, J. Appl. Phys. 105 (2009) 44907, https://doi.org/10.1063/1.3082113.
[43] L. Zhang, L. Chen, S. Xia, C. Wang, F. Sun, Entropy generation minimization for reverse water gas shift (RWGS) reactors, Entropy 20 (2018) 415, https://doi.org/10.3390/e20060415.
[44] L. Chen, M. Kang, G. Yanlin, S. Fengrui, Minimum entropy generation path for an irreversible light-driven engine with A=B reacting system and linear phenomenological heat transfer law, Environ. Eng. Manag. J. 16 (2017) 2035–2043.
[45] L. Chen, A. Yang, Z. Xie, F. Sun, Constructal entropy generation rate minimization for cylindrical pin-fin heat sinks, Int. J. Therm. Sci. 111 (2017) 168–174, https://doi.org/10.1016/j.ijthermalsci.2016.08.017.
[46] Optimal concentration configuration of consecutive chemical reaction A ⇔ B ⇔ C for minimum entropy generation, J. Non-Equilib. Thermodyn. 41 (2016) 313, https://doi.org/10.1515/jnet-2016-0009.
[47] H. Feng, L. Chen, Z. Xie, F. Sun, Constructal entropy generation rate minimization for asymmetric vascular networks in a disc-shaped body, Int. J. Heat Mass Transf. 91 (2015) 1010–1017, https://doi.org/10.1016/j.ijheatmasstransfer.2015.08.045.
[48] H. Feng, L. Chen, Z. Xie, F. Sun, "Disc-point" heat and mass transfer constructal optimization for solid–gas reactors based on entropy generation minimization, Energy 83 (2015) 431–437, https://doi.org/10.1016/j.energy.2015.02.040.
[49] Y. Ge, L. Chen, F. Sun, Optimal path of piston motion of irreversible Otto cycle for minimum entropy generation with radiative heat transfer law, J. Energy Inst. 85 (2012) 140–149, https://doi.org/10.1179/1743967112Z.00000000025.
[50] Y. Ge, L. Chen, F. Sun, Optimal Paths of Piston Motion of Irreversible Otto Cycle Heat Engines for Minimum Entropy Generation, vol. 40, 2010.
[51] M. Sheremet, I. Pop, H. Öztop, N. Abu-Hamdeh, Natural convection of nanofluid inside a wavy cavity with a non-uniform heating: entropy generation analysis, Int. J. Numer. Methods Heat Fluid Flow 27 (2017) 958–980, https://doi.org/10.1108/HFF-02-2016-0063.
[52] C.-C. Cho, C.-L. Chen, C.-K. Chen, Natural convection heat transfer and entropy generation in wavy-wall enclosure containing water-based nanofluid, Int. J. Heat Mass Transf. 61 (2013) 749–758, https://doi.org/10.1016/j.ijheatmasstransfer.2013.02.044.
[53] M. Akbarzadeh, S. Rashidi, N. Karimi, N. Omar, First and second laws of thermodynamics analysis of nanofluid flow inside a heat exchanger duct with wavy walls and a porous insert, J. Therm. Anal. Calorim. (2018)https://doi.org/10.1007/s10973-018-7044-y.
[54] M. Akbarzadeh, S. Rashidi, N. Karimi, R. Ellahi, Convection of heat and thermodynamic irreversibilities in two-phase, turbulent nanofluid flows in solar heaters by corrugated absorber plates, Adv. Powder Technol. 29 (2018) 2243–2254, https://doi.org/10.1016/j.apt.2018.06.009.
[55] J.A. Esfahani, M. Akbarzadeh, S. Rashidi, M.A. Rosen, R. Ellahi, Influences of wavy wall and nanoparticles on entropy generation over heat exchanger plat, Int. J. Heat Mass Transf. 109 (2017) 1162–1171, https://doi.org/10.1016/j.ijheatmasstransfer.2017.03.006.
[56] M. Akbarzadeh, S. Rashidi, J.A. Esfahani, Influences of corrugation profiles on entropy generation, heat transfer, pressure drop, and performance in a wavy channel, Appl. Therm. Eng. 116 (2017) 278–291, https://doi.org/10.1016/j.applthermaleng.2017.01.076.
[57] M.A. Ahmed, M.Z. Yusoff, K.C. Ng, N.H. Shuaib, The effects of wavy-wall phase shift on thermal-hydraulic performance of Al_2O_3–water nanofluid flow in sinusoidal-wavy channel, Case Stud. Therm. Eng. 4 (2014) 153–165, https://doi.org/10.1016/j.csite.2014.09.005.
[58] A. Ebrahimi-Moghadam, M. Farzaneh-Gord, M. Deymi-Dashtebayaz, Correlations for estimating natural gas leakage from above-ground and buried urban distribution pipelines, J. Nat. Gas Sci. Eng. 34 (2016) 185–196, https://doi.org/10.1016/j.jngse.2016.06.062.
[59] Ansys-Fluent 16.2 User's Guide. , ANSYS Inc., 2015
[60] M. Mahdavi, M. Sharifpur, M.H. Ahmadi, J. Meyer, Aggregation study of Brownian nanoparticles in convective phenomena, J. Therm. Anal. Calorim. (2018)https://doi.org/10.1007/s10973-018-7283-y.
[61] A. Ebrahimi-Moghadam, M. Farzaneh-Gord, A. Arabkoohsar, A.J. Moghadam, CFD analysis of natural gas emission from damaged pipelines: correlation development for leakage estimation, J. Clean. Prod. 199 (2018) 257–271, https://doi.org/10.1016/j.jclepro.2018.07.127.
[62] M. Farzaneh-Gord, M.S. Pahlevan-Zadeh, A. Ebrahimi-Moghadam, S. Rastgar, Measurement of methane emission into environment during natural gas purging process, Environ. Pollut. (2018)https://doi.org/10.1016/j.envpol.2018.07.027.
[63] A. Ebrahimi-Moghadam, M. Farzaneh Gord, M. Deimi Dasht bayaz, Develop an equation to calculate the amount of gas leakage from buried distribution gas pipelines, Iran J. Mech. Eng. 18 (2016) 64–86.
[64] B. Mohseni-Gharyehsafa, A. Ebrahimi-Moghadam, V. Okati, M. Farzaneh-Gord, M.H. Ahmadi, G. Lorenzini, Optimizing flow properties of the different nanofluids inside a circular tube by using entropy generation minimization approach, J. Therm. Anal. Calorim. (2018)https://doi.org/10.1007/s10973-018-7276-x.
[65] H.R. Ashorynejad, A. Zarghami, Magnetohydrodynamics flow and heat transfer of Cu-water nanofluid through a partially porous wavy channel, Int. J. Heat Mass Transf. 119 (2018) 247–258, https://doi.org/10.1016/j.ijheatmasstransfer.2017.11.117.
[66] D.J. Tritton, Physical Fluid Dynamics, Springer Science & Business Media, 2012https://doi.org/10.1007/978-94-009-9992-3.
[67] A. Bejan, Entropy Generation Minimization: The Method of Thermodynamic Optimization of Finite-Size Systems and Finite-Time Processes, CRC press, 1995.
[68] A. Ebrahimi-Moghadam, B. Mohseni-Gharyehsafa, M. Farzaneh-Gord, Using artificial neural network and quadratic algorithm for minimizing entropy generation of Al_2O_3-EG/W nanofluid flow inside parabolic trough solar collector, Renew. Energy 129 (Part A) (2018) 473–485, https://doi.org/10.1016/j.renene.2018.06.023.
[69] C.-C. Wang, C.-K. Chen, Forced convection in a wavy-wall channel, Int. J. Heat Mass Transf. 45 (2002) 2587–2595, https://doi.org/10.1016/S0017-9310(01)00335-0.

Nomenclature

a: wave amplitude (m)
b: wave length (m)
Be: Bejan number (−)
C: heat capacity (J/kgK)
g: gravitational acceleration (m/s^2)
Gr: Grashof number (−)
H: half of the channel height (m)
k: conductivity factor (W/mK)
L: total length of the channel (m)
N_g: volumetric entropy generation number (−)
N_s: average entropy generation number (−)
Nu: Nusselt number (−)
p: pressure (Pa)
Pr: Prandtl number (−)
Re: Reynolds number (−)
Ri: Richardson number (−)
$\dot{S}'''_{gen}$: volumetric entropy generation rate (W/m^{3}K)
T: temperature (K)
u: horizontal component of the velocity (m/s)
v: vertical component of the velocity (m/s)
$\forall$: Volume (m^3)
x: horizontal direction (m)
y: vertical direction (m)

Subscripts

0: inlet conditions
avg: average
b: bulk
f: base fluid
H: thermal
nf: nanofluid
s: nanoparticle
V: viscous
w: wall

Greek letters

α: wave amplitude ratio (−)
β: thermal expansion coefficient (1/K)
ϕ: nanoparticles volume fraction (−)
λ: wave length ratio (−)
μ: viscosity (kg/ms)
ρ: density (kg/m^3)